LETTER • OPEN ACCESS

Spectrally tunable phase-biased NALM mode-locked Yb:fiber laser with nJ-level pulse energy

IOP Publishing J. Phys. Photonics 6 (2024) 02LT01 https://doi.org/10.1088/2515-7647/ad3d1b

Journal of Physics: Photonics

OPEN ACCESS

RECEIVED
1 November 2023

REVISED
29 February 2024

ACCEPTED FOR PUBLICATION
10 April 2024

PUBLISHED
16 April 2024

LETTER

Spectrally tunable phase-biased NALM mode-locked Yb:fiber laser with nJ-level pulse energy

Saeid Ebrahimzadeh[1,*], Sakib Adnan[1], Yishen Li[1], Vito F Pecile[2,3], Jakob Fellinger[2], Sarper Salman[4,5,6], Christoph M Heyl[4,5,6], Ingmar Hartl[4], Oliver H Heckl[2] and Gil Porat[1,7]

[1] Department of Electrical and Computer Engineering, University of Alberta, Edmonton, Alberta T6G 1H9, Canada
[2] Christian Doppler Laboratory for Mid-IR Spectroscopy and Semiconductor Optics, Faculty Center for Nano Structure Research, Faculty of Physics, University of Vienna, 1090 Vienna, Austria
[3] Vienna Doctoral School in Physics, University of Vienna, 1090 Vienna, Austria
[4] Deutsches Elektronen-Synchrotron DESY, 22607 Hamburg, Germany
[5] GSI Helmholtzzentrum für Schwerionenforschung GmbH, 64291 Darmstadt, Germany
[6] Helmholtz-Institute Jena, 07743 Jena, Germany
[7] Department of Physics, University of Alberta, Edmonton, Alberta T6G 2E1, Canada
[*] Author to whom any correspondence should be addressed.

E-mail: saeid1@ualberta.ca

Keywords: mode-locked lasers, ultrafast lasers, fiber lasers

Abstract

Applications of mode-locked fiber lasers benefit from robust and self-starting mode-locking, spectral tuning, high pulse energy and high average power. All-polarization-maintaining (PM) fiber lasers mode-locked with a phase-biased nonlinear amplifying loop mirror (NALM) have been shown to be very robust and reliably self-starting, and provide either spectral tuning or high pulse energy, but not both. We report on a simple method for concurrent spectral tuning and nanojoule-level pulse energy scaling of an all-PM phase-biased NALM mode-locked Yb:fiber laser, which we demonstrate over a 54 nm tuning range, reaching up to 1.67 nJ pulse energy and 126 mW average power. Unlike other laser configurations, our results show that net normal dispersion is not necessary or optimal for scaling the pulse energy of this type of mode-locked fiber laser.

The applications of mode-locked lasers with $\sim 1\,\mu$m wavelength cover vast areas in science and industry, including micro-machining, precision metrology and spectroscopy [1]. Applications' needs have been driving the development of mode-locked ytterbium-doped (Yb-doped) fiber laser oscillators, where robustness, self-starting mode-locking, tunable wavelength, and high pulse energy and power are highly desirable. This is also true where the necessary power or pulse energy levels are available only through further amplification of the oscillator output [2–4]. However, to date, laser development has focused on one or some of these desired properties, but not all of them concurrently. Here, we address all of these issues at once. More specifically, we demonstrate, for the first time to the best of our knowledge, (i) concurrent spectral tuning and output pulse energy scaling to nJ-level in a robust self-starting phase-biased nonlinear amplifying loop mirror (NALM) mode-locked laser; (ii) the concurrent achievement of lower relative intensity noise (RIN) and higher pulse energy in the net anomalous and close-to-zero dispersion regimes in comparison to the net normal dispersion regime.

Self-starting mode-locking and its robust operation depend strongly on the method of mode-locking, involving either real or artificial saturable absorbers [5]. Real saturable absorbers include semiconductor saturable absorber mirrors, graphene, carbon nanotubes and topological insulators. Though real saturable absorbers offer self-starting and robust mode-locking, they suffer from degradation over time, complexity of fabrication and increased timing jitter [6]. These drawbacks have made artificial saturable absorbers a more common choice in mode-locking of fiber lasers. Nonlinear polarization rotation (NPR) and NALM are the most widely used artificial saturable absorbers for mode-locking fiber lasers. Since NPR relies on polarization evolution, it cannot be realized in polarization-maintaining (PM) fibers, and therefore it is highly sensitive to environmental conditions. In NALM-based mode-locking, the interference of two counter-propagating waves depends on their relative nonlinear phase shift, making the NALM's reflectivity

intensity-dependent. This mechanism can be implemented in PM fibers, so it is able to provide highly robust operation. However, initiating mode-locking in NALM lasers is difficult, because the NALM's reflectivity depends very weakly on intensity for the low intensities at the initial step of the mode-locking process. To address this issue, the NALM was phase-biased (using nonreciprocal polarization optics) such that its reflectivity quickly increases with intensity at low intensities, making it easy for noise to drive the laser into a mode-locked state, i.e. self-start mode-lock. These fiber lasers have attracted significant attention in recent years thanks to their reliable, straightforward and robust operation [7–11].

Mode-locked fiber lasers generally provide limited pulse energy, commonly on the pJ scale. Mode-locking requires a delicate balance between gain, loss, dispersion and self-phase modulation (SPM). The small mode area and meter-scale length of fibers makes SPM scale quickly with pulse energy, so the balance can only be kept for low pulse energies. However, high pulse energy seed sources are desirable in amplifier systems where they can reduce the number of amplification stages and mitigate amplified spontaneous emission. In addition, nJ-level pulses can drive coherent supercontinuum generation, e.g. for frequency comb offset frequency detection and stabilization. A mode-locked oscillator directly emitting nJ pulses can therefore drive supercontinuum generation without the need for external amplification.

There are various methods to increase the output power or energy of a mode-locked fiber laser. Operation with all-normal or net-normal intracavity dispersion has been shown to serve this purpose [12, 13]. However, such lasers exhibit increased timing jitter [14] and intensity noise [15, 16] and require high pump power. Another approach in energy-scaling uses large-mode-area (LMA) fibers. Pulse energy as high as 28 nJ using PM-LMA fiber has been recently realized [17]. With LMA fibers, special care is needed to suppress high order modes to achieve and maintain mode-locking and good beam quality [18]. In addition, coupling light into LMA fibers requires sensitive and critical free-space alignment, limiting their robustness. To the best of our knowledge, only one method has been shown to systematically increase the output power and pulse energy of a phase-biased NALM laser, as demonstrated with an erbium-doped fiber laser [8]. In this technique, intracavity waveplates orientations and pump power are adjusted in an iterative stepwise manner, involving dozens of precise and carefully timed steps realized via computer control. This process keeps the laser mode-locked as the phase bias is gradually shifted to support higher pulse energy. Though this approach can be used with Yb-doped fiber lasers as well, it is very complex and time-consuming.

For an overview of mode-locked fiber laser spectral tuning techniques, we refer the reader to Zhao *et al* [19]. The only method we are aware of that has been demonstrated to spectrally tune a phase-biased NALM laser is by rotating a mirror behind the intracavity grating pair [9, 10]. In a configuration utilizing a double-clad Yb-doped gain fiber, with the phase bias applied in the NALM loop so that the grating pair and tilted mirror were directly behind a fiber collimator, it provided tuning over 1034–1104 nm [10]. When implemented in a laser with single-clad gain fiber, where the phase bias was applied in the free space section (same as shown in figure 1), the same method yielded tuning over 1015–1105 nm [9]. However, we observed that such tilting is accompanied by misalignment of the output beam, and in both cases operation was limited to low average output power ($\leqslant$15 mW) and pJ pulse energy.

To the best of our knowledge, the concurrent ability to scale energy and tune optical spectra in phase-biased NALM lasers has not been studied. In this paper, we present a self-starting all-PM phase-biased NALM mode-locked fiber laser with a simple method for concurrent energy scaling and spectral tuning. We tune the output wavelength by translating a slit behind a grating pair, and scale the output pulse energy by simply rotating an intracavity waveplate that controls output coupling loss. For some wavelengths, we obtain additional gain in pulse energy by also increasing the pump power. We achieved an overall tuning range from 1017 nm to 1071 nm, recording nJ-level output pulse energies throughout nearly the entire range. Additionally, we successfully scaled the output pulse energy to over 1.3 nJ in the net-anomalous, close-to-zero and net-normal dispersion regimes. Interestingly, our laser delivers higher pulse energy and power and lower RIN with near-zero dispersion than with net-normal dispersion. Therefore, our results indicate that net-normal dispersion does not provide any advantage to energy scaling of phase-biased NALM lasers.

Figure 1 shows the schematic of the laser setup. The pump diode is a 976 nm fiber Bragg grating-stabilized diode laser (3SPTechnologies 1999CVB). The loop consists of a polarization beam combiner and collimator (PBCC), a wavelength division multiplexer (WDM) and a 49 cm PM active fiber (CorActive Yb-401PM). This length of active fiber was chosen for convenience of splicing $\sim$50 cm fibers with our fiber fusion splicer (Fujikura FSM-100P). The passive PM fiber (Thorlabs PM980 XP) in the loop has a total length of 176 cm. Since the two ports of the PBCC have orthogonal orientations, the fiber inside the loop is twisted by 90° to match them. A 45° Faraday rotator (FR), a quarter waveplate (QWP) and a half waveplate (HWP1) comprise the nonreciprocal phase shifting components. The remainder of the laser oscillator is made of a polarization beam splitter (PBS), half wave plate (HWP2), grating pair (LightSmyth T-1000-1040-3212-94) with 1000 lines mm^{-1}, and a protected silver end-mirror.

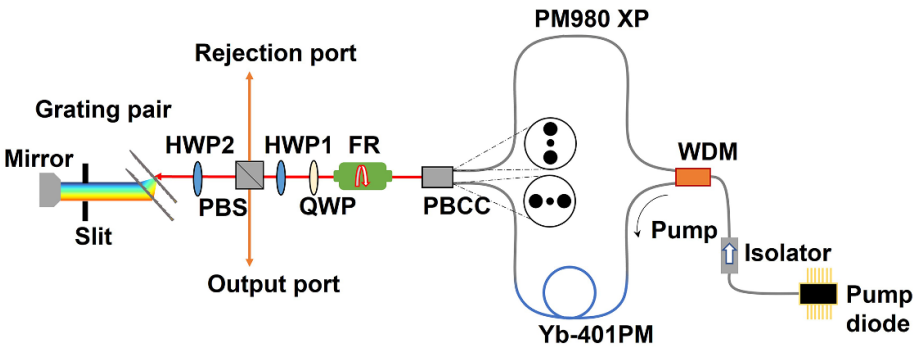

Figure 1. Schematic diagram of the laser.

To achieve mode-locking, the two pulses that counter-propagate through the loop interfere at the PBS. QWP and HWP1 are set such that high-intensity light is transmitted through the PBS after accumulating sufficient nonlinear phase shift in the loop, while the low intensity light is reflected into the rejection port [20]. Hence, the rejected light is a measure of nonlinear (saturable) loss in the cavity. HWP2 controls the output coupling rate (contributing to linear, non-saturable loss) of the pulses after a round-trip through the grating pair, facilitated by reflection off the end-mirror. The grating pair separation controls the net dispersion in the cavity. We have inserted a slit behind the grating pair for spectral tuning via filtering the dispersed beam.

In our experiment, we always begin with the waveplates orientations set for self-starting mode-locking when turning on the pump laser: HWP1 at 29 degrees, QWP at 78 degrees, and HWP2 at 2–3 degrees. All the angles of waveplates orientations we report are the angles of the fast axes of the waveplates with respect to the horizontal. For net anomalous or near-zero dispersion, the pump power was set to 219 mW, while for net positive dispersion it was set to 256 mW. We measured the intracavity dispersion for each operation point using the method of Knox [21]. After mode-locking, we translate a slit across the dispersed beam immediately behind the grating pair (see figure 1) to tune the center wavelength and bandwidth. Mode-locking is lost beyond a certain range of translation in either direction, thereby setting the wavelength tuning range. Most likely, the tuning range is limited by the spectral properties of the WDM. Outside this tuning range the WDM produces high intracavity loss that hampers mode-locking, and also has higher transmission of light from the cavity to the pump laser (protected by an isolator for 976 nm) that destabilizes the pump laser operation.

Figure 2 shows the spectral tuning of the laser output at different dispersion regimes. Figures 2(a), (d), and (g) show the optical spectra at grating separations of 18.4 mm, 12.9 mm, and 7.5 mm, respectively (measured with an Ando AQ6317 optical spectrum analyzer with 1 nm resolution bandwidth (RBW)), providing wavelength tuning over 1017–1064 nm, 1021–1071 nm, and 1023–1066 nm, respectively. The group delay dispersion (GDD) corresponding to each curve is indicated above it. GDD values range from $-0.074\ \mathrm{ps}^2$, through $0.0057\ \mathrm{ps}^2$ to $0.026\ \mathrm{ps}^2$, corresponding to laser operation from the net-anomalous, through near-zero, to the net-normal dispersion regime. The presence of Kelly sidebands [22] in figure 2(a) signifies soliton mode-locking when the net dispersion is anomalous, as expected. In the short wavelength side of figure 2(d), and the long wavelength side of figure 2(g) the laser is operating with near-zero net dispersion, i.e. stretched-pulse mode-locking. Lastly, in the short wavelength side in figure 2(g) the laser is in the net-normal dispersion regime, i.e. disspative soliton mode-locking.

Figures 2(b), (e), and (h) display the fundamental harmonic of the RF spectrum offset to zero, when the central wavelengths were 1023 nm, 1044 nm, and 1023 nm, respectively. The data was taken with a Newport Si 1601FS-AC photoreceiver with bandwidth of 1 GHz and Signal Hound USB-SA44B spectrum analyzer set to an RBW of 30 Hz. At grating separations of 18.4 mm, 12.9 mm and 7.5 mm, the repetition rates were 75.1 MHz, 75.3 MHz and 75.6 MHz, respectively. The signal-to-noise ratio was more than 90 dB for all cases. Figure 2(c), (f) and (i) show the higher RF harmonics (taken with the same photoreceiver and an Agilent E4411B RF spectrum analyzer set to an RBW of 10 kHz) of the laser output at the corresponding states, demonstrating clean and stable mode-locked operation.

In a second experiment, in addition to the steps outlined above, we increased the pump power and adjusted the output coupling by rotating HWP2, such that output power was maximized. Further increasing the pump power or output coupling resulted in loss of mode-locking, multi-pulsing, or continuous wave (CW) breakthrough. Note that the laser still self-start mode-locked with HWP2 oriented at approximately

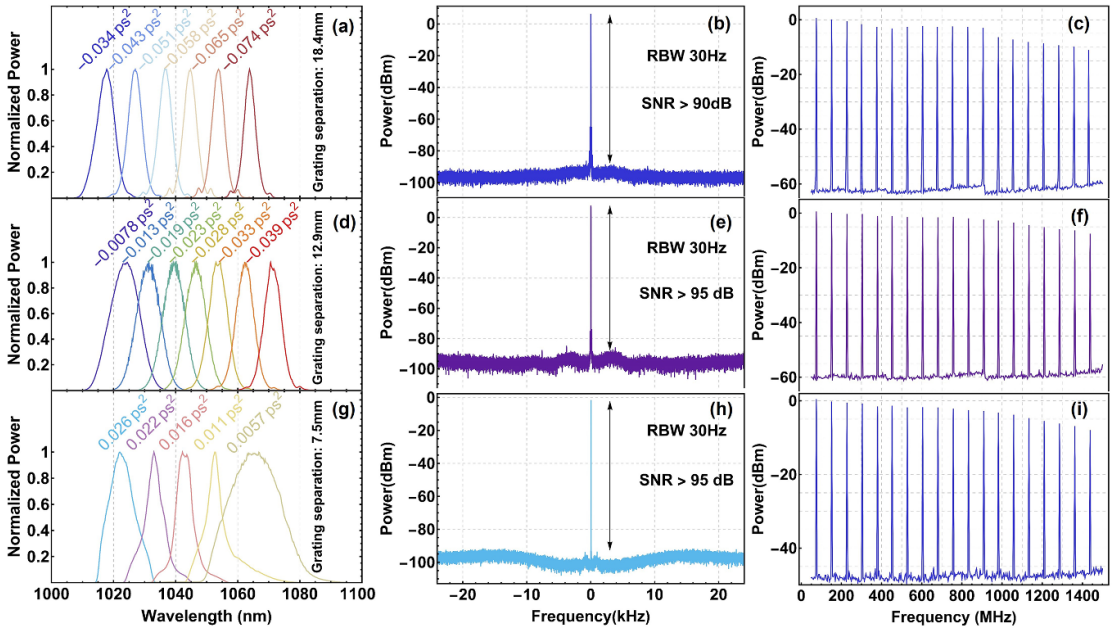

Figure 2. Optical and RF spectra of the laser output with HWP2 at 2–3 degrees and grating separation of 18.4 mm (a)–(c), 12.9 mm (d)–(f) and 7.5 mm (g)–(i).

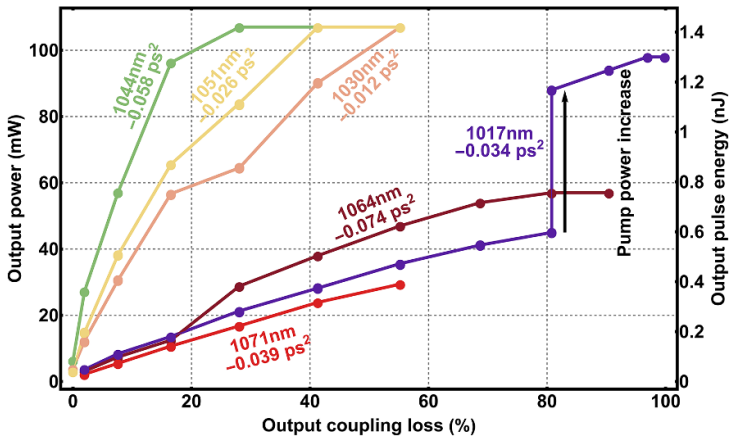

Figure 3. Highest obtained output power values (left scale) and pulse energy (right scale) vs. output coupling loss at five different wavelengths and GDD values.

2 degrees (∼2% outcoupling loss). This low output coupling is crucial for self-starting, since it makes the intracavity transmission curve strongly depend on intracavity power when the power is low, i.e. when the nonlinear phase shift difference is small. Note that we define the outcoupling loss as the fraction of optical power reflected by the PBS into the output port, and we calculate it using Jones matrix calculus [7].

Here we detail the procedure that led to maximum output power with clean mode-locking for each center wavelength. Following mode-locking, for center wavelengths of 1030 nm, 1044 nm, 1051 nm and 1071 nm the maximum pump power was ∼253 mW, and at 1064 nm we increased the pump power to ∼265 mW. Next, we rotated HWP2. In the case of 1017 nm, though, we started with a pump power of ∼156 mW. Next, we increased the outcoupling loss to ∼80% (HWP2 angle of ∼16 degrees) and followed with gradually increasing the pump power to 252 mW in increments of ∼24 mW. Finally, we increased the loss to ∼99% (HWP2 angle of ∼22 degrees).

Figure 3 shows the output power (left scale) and output pulse energy (right scale) as a function of output coupling loss. Overall, we achieved output power of 110 mW (pulse energy of 1.42 nJ) for center wavelengths of 1030 nm, 1044 nm and 1051 nm, and output power (pulse energy) of 98 mW (1.3 nJ), 57 mW (0.75 nJ) and 30 mW (0.4 nJ) for 1017 nm, 1064 nm and 1071 nm, respectively. The GDD values corresponding to the center wavelengths of 1017 nm, 1030 nm, 1044 nm, 1051 nm, 1064 nm and 1071 nm are $-0.034\ \mathrm{ps}^2$, $-0.012\ \mathrm{ps}^2$, $-0.058\ \mathrm{ps}^2$, $-0.026\ \mathrm{ps}^2$, $-0.074\ \mathrm{ps}^2$ and $-0.039\ \mathrm{ps}^2$, respectively. The maximum pump power in

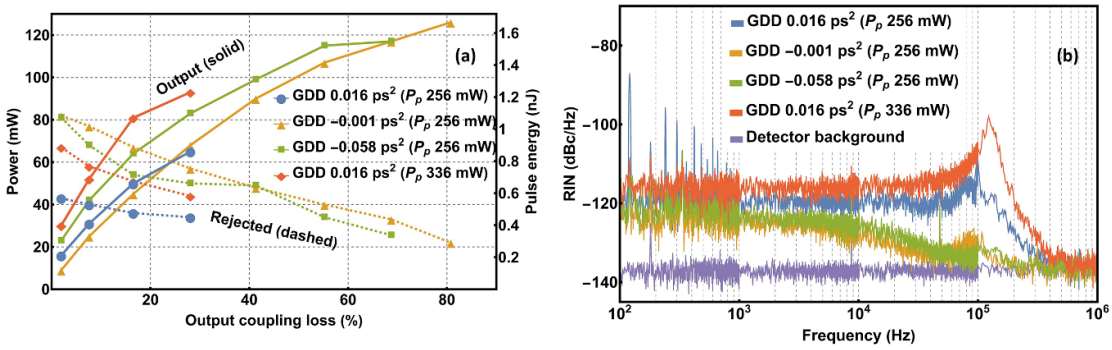

Figure 4. Output (solid) and rejected (dashed) power and pulse energy (a) and output port RIN measurements at maximum output power (b) for center wavelength of 1044 nm and different GDD and pump power (P_p) values.

each case was ∼256 mW. The Yb:fiber emission cross section is similar for wavelengths in the range 1017–1051 nm, while it is significantly lower for 1064 nm and 1071 nm. We attribute the lower maximum power at 1064 nm and 1071 nm to the lower gain at these wavelengths.

The data presented in figure 3 is a subset of the all the power scaling attempts at different center wavelengths and GDD values. It shows the highest power obtained at each wavelength over three dispersion values, corresponding to the three gratings separations. Notably, in all cases, the highest power was obtained with net anomalous dispersion.

We conducted a third experiment to discern the role of dispersion in the power scaling mechanism. We mode-locked the laser in the same manner as described above, but kept the center wavelength and pump power fixed at 1044 nm and 256 mW, respectively, and varied the net cavity dispersion by adjusting the grating pair separation. We took extra care to set the net dispersion very close to zero in one case. Then, for each dispersion regime, we rotated HWP2 to increase the output power.

Figure 4(a) shows the output (solid lines) power and rejected (dashed lines) power on the left scale and corresponding pulse energy on the right scale as a function of output coupling loss. We recorded a maximum output power (pulse energy) of 65 mW (0.8 nJ), 126 mW (1.67 nJ) and 117 mW (1.55 nJ) for net intracavity GDD of 0.016 ps^2, −0.001 ps^2 and −0.058 ps^2, respectively. The red curves with diamond markers are for GDD of 0.016 ps^2 with pump power of 336 mW, which was the highest pump power at which clean mode-locking was maintained for this GDD with HWP at ∼2 degrees, i.e. in the self-starting condition. In this case, the output power was 93 mW, corresponding to pulse energy of 1.23 nJ. We were able to further increase the pulse energy to 1.33 nJ (corresponding to output power of 101 mW) when we increased the pump power to 363 mW while the output coupling loss was 28%.

For all three dispersion values in figure 4(a), as outcoupling loss increases, output power increases and rejected power decreases. These observations indicate that when linear loss is increased, the laser reduces the nonlinear loss to maintain mode-locking [23]. We could not maintain mode-locking for output coupling losses higher than about 28%, 80% and 70% in the dissipative soliton, stretched-pulse and soliton regimes, respectively. Therefore, with the same pump power, we observe a much lower tolerance to outcoupling loss in the net-normal dispersion regime than in the other cases. Correspondingly, we achieve the highest output power and pulse energy with near zero net dispersion, where net anomalous dispersion yields only slightly lower values, and both are almost double the results obtained with net normal dispersion and the same pump power. Even when we increased the pump power as much as possible while maintaining stable mode-locking, net-normal dispersion yielded ∼20% lower output power.

We attribute the greater output pulse energy scaling in the soliton and stretched-pulse regimes, as compared to the dissipative soliton regime, to the nonlinear loss mechanism involved in dissipative soliton mode-locking. With net-anomalous or near-zero dispersion, a phase-biased NALM laser can operate with lower intracavity pulse energy (as compared to a non-phase-biased NALM laser) and still have enough SPM for mode-locked operation [24]. Therefore, it can maintain mode-locking with higher outcoupling loss and provide higher output pulse energy. In dissipative soliton mode-locking, normal dispersion and SPM combine to produce strongly chirped and stretched pulses that get spectrally filtered (e.g. via gain dispersion) to facilitate mode-locking [13], which still requires high intracavity pulse energy. Moreover, the stretched intracavity pulse is longer, meaning that higher energy is necessary to reach the same intensity and the same level of SPM. Therefore, dissipative soliton mode-locking can tolerate a lower level of outcoupling loss than soliton and stretched-pulse mode-locking, and is thus less amenable to output pulse energy scaling by increasing outcoupling loss.

Table 1. GDD, pump power, output power, output pulse energy and RMS RIN integrated over 100 Hz–1 MHz corresponding to the data in figure 4(b).

GDD (ps^2)	Pump power (mW)	Output power (mW)	Output pulse energy (nJ)	RMS RIN (%)
0.016	256	65	0.8	0.066
−0.001	256	126	1.67	0.019
−0.058	256	117	1.55	0.02
0.016	336	93	1.23	0.22

We note that a previous experiment by Liu *et al* [17], utilizing free-space coupling into an LMA Yb-doped fiber in a phase-biased NALM laser, achieved higher pulse energy with all-normal dispersion (ANDi) than with close-to-zero net dispersion. In that experiment, when a grating pair was used to control intracavity dispersion, outcoupling was optimized using a QWP behind the grating pair, and not an HWP in front of it, as we do here. We note that gratings also transform the polarization state. For example, the grating pair used in our laser behaves as a quarter wave plate, as described by Mayer *et al* [7]. Therefore, we suspect that the outcoupling optimization method of Liu *et al* inadvertently introduced additional loss. Indeed, the authors report that mode-locking was achieved only for net cavity dispersion of $-0.056\ ps^2$ to $0.002\ ps^2$, i.e. in the net anomalous and near-zero regimes, but not in the net-positive regime, as would be the case if intracavity losses are too high (our results also demonstrated the vulnerability of mode-locking in the net-normal regime to loss; see figure 4(a)). Furthermore, for operation in the ANDi regime, Liu *et al* removed the grating and QWP and replaced them with a spectral filter, which was preceded by a PBS and HWP that allowed to fully control and optimize the outcoupling loss. Therefore, the results presented by Liu *et al* do not exclude the possibility of achieving higher pulse energy with close-to-zero net dispersion, should they use the same outcoupling optimization method presented here.

We also investigated the impact of dispersion on RIN at different dispersion regimes in high-power operation. Figure 4(b) shows measured RIN at the maximum output power for each GDD value presented in figure 4(a). These data were taken with a Thorlabs DET08C photodetector connected to a low pass filter (Mini-Circuits BLP 1.9+) and a home-made DC block that protected a Signal Hound USB-SA44B spectrum analyzer. Table 1 details the measurement conditions employed in figure 4(b), and the corresponding RIN integrated over 100 Hz to 1 MHz. With pump power of 256 mW, we achieved the lowest RIN in the close-to-zero dispersion regime with integrated RIN of 0.019%, and also the highest output power and pulse energy, 126 mW and 1.67 nJ, respectively. The negative dispersion regime yielded very similar results, with only slightly lower power and higher RIN. With the same pump power, the integrated RIN in the net-normal dispersion regime was 0.066%, while the output power and pulse energy were 65 mW and 0.8 nJ, respectively. Increasing the pump power to 336 mW also increased the integrated RIN to 0.22% and the output power and pulse energy to 93 mW and 1.23 nJ, respectively. Therefore, at close-to-zero dispersion regime, we not only obtained the highest output power, but also the lowest RIN. We note that the RIN data in figure 4(b) shows a peak near 100 kHz, which increases by about 20 dB when the pump power is increased. Although the peak at 100 kHz is evident in all our RIN spectra, it is most pronounced in the net-normal dispersion regime, particularly at a pump power of 336 mW. While it has been previously established that near-zero dispersion yields optimal RIN performance [15, 16], as we observe here, achieving both superior output power and RIN performance in this regime as compared to net-normal dispersion is a novelty of the phase-biased NALM laser.

We propose the following as a possible explanation for the RIN trends we observe, based on the model established by Newbury *et al* [25, 26], which we summarize here. Pump-to-output noise transfer is effectively low-pass filtered by the interplay between gain saturation and saturation of self-amplitude modulation (SAM). The latter refers to an increase in nonlinear loss with increasing intracavity pulse energy. Stronger saturation of SAM, i.e. a higher rate of increase of loss with pulse energy, leads to a smaller bandwidth of the low-pass filtering effect, and therefore greater attenuation of pump-to-output noise transfer, and lower output RIN. In our laser, in all dispersion regimes, variation in saturable absorption results from variation in SPM. A shorter pulse will experience a greater variation in SPM for the same variation in pulse energy, and therefore stronger saturation of SAM that produces lower RIN. Since dissipative soliton mode-locking relies on strongly stretched pulses, it will result in higher RIN than soliton and stretched-pulse mode-locking, as we observe. Particularly, we suggest that the RIN peak around 100 kHz originates from pump-to-output noise transfer. This peak is more strongly suppressed by the filtering effect in the soliton and stretched-pulse regimes than in the dissipative soliton regime. When we increased the pump power in the dissipative soliton regime, pump noise around 100 kHz increased, resulting in a corresponding increase in RIN around the same frequency.

To conclude, we have demonstrated concurrent energy scaling and spectral tuning of a phase-biased NALM mode-locked Yb:fiber laser. Particularly, we have shown a wavelength tuning range of 54 nm, from 1017 nm to 1071 nm, with nJ-level pulse energy. Furthermore, we achieved nJ energy levels in the three regimes of soliton (1.55 nJ), stretched-pulse (1.67 nJ) and disspative soliton (1.33 nJ) mode-locking, where pump power did not limit further energy scaling. Additionally, the lowest output RIN concurred with the highest pulse energy of the stretched-pulse regime, thereby showing that net-normal dispersion is not necessary or optimal when aiming for high pulse energy with this type of laser. Our results show the suitability of this laser for a variety of applications, most particularly as seed source for chirped-pulse amplification systems.

Data availability statement

The data cannot be made publicly available upon publication because they are not available in a format that is sufficiently accessible or reusable by other researchers. The data that support the findings of this study are available upon reasonable request from the authors.

Acknowledgments

We acknowledge the support of the Natural Sciences and Engineering Research Council of Canada (NSERC), (Funding Reference Number RGPIN-2019-05017), the Government of Canada's New Frontiers in Research Fund, (NFRFE-2018-01220), NSERC Alliance-Alberta Innovates Advance (570922-21 and 212200789), Canada Foundation for Innovation John R Evans Leaders Fund (40464), and the Government of Alberta's Small Equipment Grant (JEI-RCP-21-003-SEG), Quantum Major Innovation Fund Project (RCP-19-004-MIF), Quantum City (1059845-10), the Austrian Federal Ministry of Labour and Economy, the National Foundation for Research, Technology and Development, the Christian Doppler Research Association and the Austrian Science Fund, FWF (P 33680, P 36040, T 1216N, ZK 91).

ORCID iDs

Saeid Ebrahimzadeh https://orcid.org/0009-0007-0766-2081
Vito F Pecile https://orcid.org/0000-0002-1420-7948

References

[1] Fermann M E and Hartl I 2013 *Nat. Photon.* **7** 868–74
[2] Shumakova V *et al* 2022 *Photon. Res.* **10** 2309
[3] Hua Y *et al* 2018 *Opt. Lett.* **43** 1686
[4] Stark H, Buldt J, Müller M, Klenke A and Limpert J 2021 *Opt. Lett.* **46** 969
[5] Han Y, Guo Y, Gao B, Ma C, Zhang R and Zhang H 2020 *Prog. Quantum Electron.* **71** 100264
[6] Kim C, Jung K, Kieu K and Kim J 2012 *Opt. Express* **20** 29524
[7] Mayer A S *et al* 2020 *Opt. Express* **28** 18946
[8] Duan D, Wang J, Wu Y, Ma J and Mao Q 2020 *Opt. Express* **28** 33603
[9] Gao G, Wang S, Zhao Q, Cong Z, Liu Z and Zhao Z 2022 *Opt. Lett.* **47** 5869
[10] Gao K, Liu Y, Qiao W, Song Y, Zhao X, Wang A and Li T 2022 *Opt. Lett.* **47** 5
[11] Pecile V F, Mayer A S, Ballentin J K C and Heckl O H 2023 *Opt. Express* **31** 36824
[12] Runge A F J, Aguergaray C, Provo R, Erkintalo M and Broderick N G R 2014 *Opt. Fiber Technol.* **20** 657–65
[13] Renninger W H, Chong A and Wise F W 2012 *IEEE J. Sel. Top. Quantum Electron.* **18** 389–98
[14] Song Y, Jung K and Kim J 2011 *Opt. Lett.* **36** 1761
[15] Song Y, Kim C, Jung K, Kim H and Kim J 2011 *Opt. Express* **19** 14518
[16] Nugent-Glandorf L, Johnson T A, Kobayashi Y and Diddams S A 2011 *Opt. Lett.* **36** 1578
[17] Liu W, Shi H, Cui J, Xie C, Song Y, Wang C and Hu M 2018 *Opt. Lett.* **43** 2848
[18] Ding E, Lefrancois S, Kutz J N and Wise F W 2011 *IEEE J. Quantum Electron.* **47** 597–606
[19] Zhao K, Yan W, Liu M, Wang L, Li H, Zhang M, Jia Z, Zhai R and Liu M 2022 *Opt. Laser Technol.* **148** 107764
[20] Li Y, Kuse N, Rolland A, Stepanenko Y, Radzewicz C and Fermann M E 2017 *Opt. Express* **25** 18017
[21] Knox W H 1994 *Appl. Phys.* B **58** 225–35
[22] Pandit N, Noske D U, Kelly S M J and Taylor J R 1992 *Electron. Lett.* **28** 455
[23] Tamura K and Nakazawa M 1995 *Appl. Phys. Lett.* **67** 3691
[24] Hänsel W *et al* 2017 *Appl. Phys.* B **123** 331–40
[25] Newbury N and Washburn B 2005 *IEEE J. Quantum Electron.* **41** 1388–402
[26] Washburn B R, Swann W C and Newbury N R 2005 *Opt. Express* **13** 10622